Separation Science and Technology
Publication details, including instructions for authors and subscription information:
http://www.informaworld.com/smpp/title~content=t713708471

Characterization of Cathodically Deposited Nickel Hexacyanoferrate for Electrochemically Switched Ion Exchange

Kavita M. Jeerage[a]; Daniel T. Schwartz[a]
[a] DEPARTMENT OF CHEMICAL ENGINEERING, UNIVERSITY OF WASHINGTON, SEATTLE, WASHINGTON, USA

Online publication date: 27 November 2000

To cite this Article Jeerage, Kavita M. and Schwartz, Daniel T.(2000) 'Characterization of Cathodically Deposited Nickel Hexacyanoferrate for Electrochemically Switched Ion Exchange', Separation Science and Technology, 35: 15, 2375 — 2392
To link to this Article: DOI: 10.1081/SS-100102344
URL: http://dx.doi.org/10.1081/SS-100102344

SEPARATION SCIENCE AND TECHNOLOGY, **35**(15), pp. 2375–2392, 2000

Characterization of Cathodically Deposited Nickel Hexacyanoferrate for Electrochemically Switched Ion Exchange

KAVITA M. JEERAGE and DANIEL T. SCHWARTZ*
DEPARTMENT OF CHEMICAL ENGINEERING
BOX 351750
UNIVERSITY OF WASHINGTON
SEATTLE, WASHINGTON 98195-1750, USA

ABSTRACT

Thin films of cathodically deposited nickel hexacyanoferrate are investigated as electrochemically switched ion-exchange (ESIX) materials for the selective separation of alkali cations in aqueous nitrate solutions at room temperature. Potential cycling in the range -100 to 900 mV vs SCE is used to reversibly load and elute alkali cations. Electrochemical cyclic voltammetry is combined with thin-film energy-dispersive x-ray spectroscopy to nondestructively determine element-specific cation loading in the ion-exchange matrix. Selectivity parameters are reported for the alkali cation pair Cs^+/Na^+. Separation factors and distribution coefficients for Cs^+ in the presence of excess Na^+ are determined over the range $[Na^+]/[Cs^+] = 10^1 - 10^6$. The distribution coefficient for cathodically deposited nickel hexacyanoferrate is greater than 2×10^5 mL/g for $[Cs^+] = 10^{-6}$ M and $[Na^+] \approx 1$ M, which is comparable in magnitude to the bulk metal hexacyanoferrates used in conventional ion exchange. A comparison between cathodically deposited nickel hexacyanoferrate materials and anodically derivatized materials is described. We also show that the Cs-form of the matrix can be electrochemically regenerated to the Na-form with nearly 80% of the intercalated Cs^+ removed.

INTRODUCTION

Metal hexacyanoferrates show promise as environmentally benign ion exchangers (1, 2). These Prussian Blue analogues contain electrochemically reversible iron centers that switch between the ferrous and ferric oxidation states

* To whom correspondence should be addressed.

depending on applied potential. Electrochemical reduction requires cation intercalation, whereas oxidation requires cation expulsion, in both cases to maintain charge neutrality within the metal hexacyanoferrate matrix. Since electrochemical rather than chemical potential (i.e. solution concentration) modulation is the main driving force for exchange, chemical regeneration of the ion-exchange matrix is not necessary. Eliminating secondary waste created by chemical regenerants and associated rinse water makes these ion exchangers more environmentally benign. For nickel hexacyanoferrate (NiHCF), the reversible cation-exchange reaction is written

$$A\mathrm{Ni^{II}Fe^{III}(CN)_6} + x\mathrm{e^-} + xA^+ \leftrightarrow \mathrm{A_{1+x}Ni^{II}Fe^{III-x}(CN)_6} \qquad (1)$$

where A^+ is the intercalated cation and x is the fractional oxidation state of the electroactive film. Note that A^+ is written as a monovalent cation; NiHCF is an excellent exchanger for alkali cations, but has a modest ability to intercalate cations from other groups in the periodic table (3). Equation (1) shows that electrochemically switched ion exchange requires a matrix with both electronic and ionic conductivity. Because NiHCF compounds are semiconductors, it is not possible to modulate the oxidation state of the iron centers in bulk materials. Instead, thin layers are grown onto a conductive substrate.

Bulk hexacyanoferrates have been widely studied as traditional ion-exchange materials for the removal of ^{137}Cs and ^{134}Cs from aqueous waste streams owing to their strong affinity for Cs^+ (4–11). However, because of the irreversibility of Cs^+ fixation (12), regenerants that remove Cs^+ from bulk hexacyanoferrates tend to degrade the ion-exchange material as well (5). Furthermore, even strong regenerants such as nitric acid (13), mercury nitrate (10), or thallium nitrate (10) do not remove all the Cs^+. Since incomplete Cs^+ removal and material degradation adversely affect further exchanger use, bulk hexacyanoferrate exchangers are currently designed for single use (5).

Thin-film NiHCF electrodes have been previously studied for ion-sensor (14, 15), electrocatalytic (16–18), as well as ion-exchange (1, 2, 19, 20) applications. Cyclic voltammetry has been used to establish the qualitative selectivity order $Cs^+ > K^+ > Na^+$ for anodically derivatized NiHCF electrodes. This result was attributed to Cs^+ being the smallest alkali cation when waters of hydration are considered (21). Water uptake does indeed accompany Li^+, Na^+, and K^+ intercalation (19). However, when Cs^+ intercalates, water is expelled (22). Furthermore, a comparison of matrix dimensions and bare cation sizes (using hard-sphere approximations) yields the same qualitative selectivity order (20). Although rather surprising, no quantitative selectivity coefficients had been determined for NiHCF thin films until very recently. Rassat et al. have reported selectivities for the binary pairs K^+/Na^+ and Cs^+/Na^+ in anodically derivatized NiHCF electrodes (2). Their studies utilized simultaneous electrochemical and quartz crystal microbalance (QCM)

measurements to determine separation factors for various solution compositions. The authors point out that variability in the apparent molar masses measured by QCM placed a limit on the range of solution compositions that could be examined.

The work of Rassat et al. utilized NiHCF films prepared by anodic derivatization of a nickel surface, in which a film forms upon dissolution of a nickel substrate in the presence of ferricyanide anions (17, 23). An alternative strategy is to cathodically deposit NiHCF films onto a conductive substrate. The film forms via reduction of ferricyanide from marginally stable solutions containing divalent nickel (19). Ion-exchange capacities for cathodically deposited films are normally much greater than those for anodically derivatized films, making them desirable for separations. Moreover, other differences might exist between cathodically deposited and anodically derivatized NiHCF films. Bulk NiHCF materials can be made with widely varied stoichiometries and properties, depending on the proportions of divalent nickel and ferricyanide in solution and how they are precipitated (12); it is a reasonable hypothesis that thin-film NiHCF electrodes prepared by anodic and cathodic methods may display different cation-exchange behaviors. There do not appear to be any reported measurements of quantitative selectivity parameters for cathodically deposited NiHCF electrodes.

This paper demonstrates a new combined energy-dispersive x-ray spectroscopy–electrochemical technique for determining quantitative selectivity values for NiHCF thin films. Our method is an ex situ technique similar to previous work that used x-ray photoelectron spectroscopy to qualitatively evaluate anion partition coefficients in conductive polymer films (24); however, as shown here, quantitative analysis of thicker films ($>$10 nm) can be accomplished without destructive sputtering. This method is demonstrated by quantifying the ion-exchange performance of cathodically deposited NiHCF electrodes loaded and eluted in various Na^+ and Cs^+ nitrate solutions. The described x-ray spectroscopy–electrochemical method has several desirable features, including the ability to probe elemental composition unambiguously, to examine ion loading from a wide range of solution compositions, and to provide local as well as spatially averaged information. Moreover, the method described here has the ability to examine thin-film NiHCF electrodes loaded with multicomponent mixtures of cations, and to quantify the cation content of the ion-exchange matrix in the reduced (fully loaded) and oxidized (theoretically half-loaded) forms. These latter attributes will be highlighted in a future publication. Selectivity parameters for cathodically deposited films are compared with those reported by Rassat et al. for anodically derivatized films and with values reported by others for traditional bulk hexacyanoferrate materials. The characteristics of electrochemical regeneration of the Cs-loaded matrix are also briefly explored.

EXPERIMENTAL

All electrochemical studies employed a PAR 273A potentiostat controlled by custom LabVIEW software. A platinum disc electrode of 5-mm diameter and 1-mm thickness was mounted to an aluminum rod and suspended such that the various electrolyte solutions wet a single (0.196-cm^2) face. A platinum wire was used as the counterelectrode and all reported potentials are referenced to a saturated calomel electrode. Energy-dispersive x-ray spectroscopy (EDS) studies employed a Link Systems Si(Li) detector attached to a JEOL JSM-5200 scanning electron microscope. Each spectrum was acquired for 10 minutes using a 15 keV electron beam to excite a 1000×1000 μm region (~5% of the exchanger area).

Prior to the cathodic deposition of a NiHCF film, the platinum electrode surface was electrochemically cleaned by cycling the potential between −275 and +1675 mV at 100 mV/sec in 1.0 M H_2SO_4. NiHCF deposition on the platinum electrode was accomplished by cycling the electrode potential between +850 and 0 mV at 25 mV/sec in freshly prepared 0.002 M $NiSO_4$, 0.002 M $K_3Fe(CN)_6$, and 0.25 M Na_2SO_4. Twenty five deposition cycles were used. The film was then thoroughly rinsed with deionized water and dried.

Cation selectivity experiments were performed by electrochemical oxidation and reduction (cyclic voltammetry) of the NiHCF electrode in various aqueous mixtures of Cs^+ and Na^+ nitrate. After cycling the potential between −100 and +900 mV for 50 times (at 50 mV/sec) in a solution of interest, the electrode was emersed while held at −100 mV. The electrode was then immersed in deionized water ≈30 seconds to remove any electrolyte dragout, dried, and x-ray spectra were acquired. (This sample-handling procedure was repeatedly found to cause less than 2% of the NiHCF to spontaneously re-oxidize, as determined by measuring the cathodic charge upon reimmersion at −100 mV.) Since it is known that NiHCF is more selective for Cs^+ than Na^+, the first solution examined was pure 1.0 M $NaNO_3$. This was followed by a sequence of mixtures containing 1 M total alkali cation concentration ($[Cs^+] + [Na^+]$) with increasing quantities of $CsNO_3$ (spaced each decade) from 10^{-7} M to 10^{-1} M. Thus, the mixture with the lowest Cs^+ composition was 10^{-7} M Cs^+ and ≈1 M Na^+, whereas the mixture with the highest Cs^+ composition was 0.1 M Cs^+ and 0.9 M Na^+. A solution containing pure 1.0 M $CsNO_3$ was examined at the end.

RESULTS AND DISCUSSION

NiHCF Deposition

Figure 1a shows cyclic voltammograms of the film deposition process. The reversible ion-exchange capacity was determined from the average of

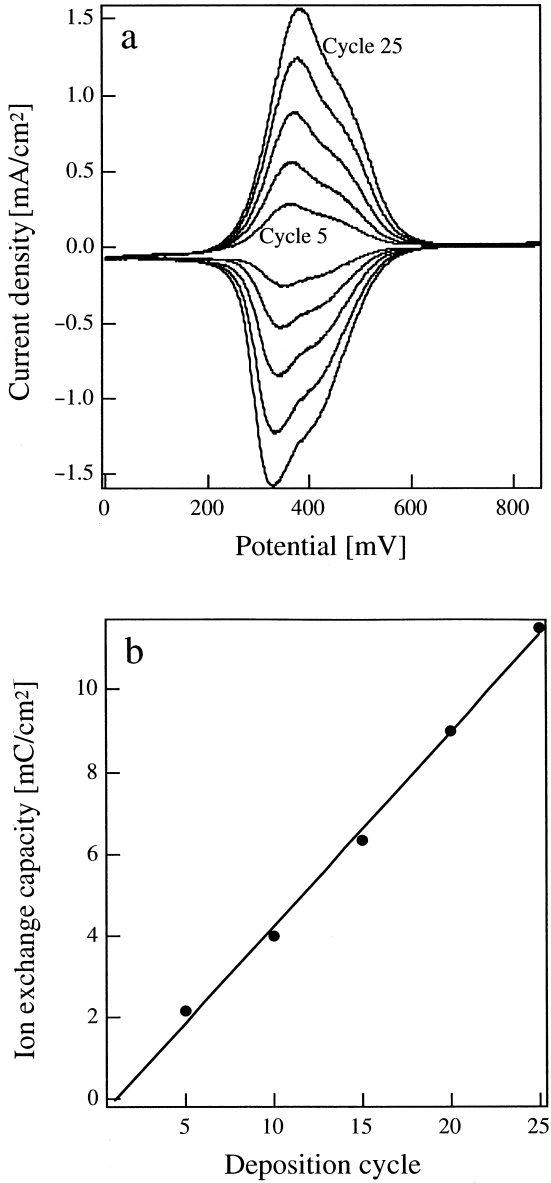

FIG. 1 Characteristics of the cathodic deposition of NiHCF. (a) Cyclic voltammograms of the film deposition process are shown every 5th cycle. (b) The reversible ion-exchange capacity grows linearly with deposition cycle number over all 25 cycles used.

the integrated charge during the anodic and cathodic sweeps of the cyclic voltammogram. The equivalent film thickness was calculated by assuming a fully redox-active cubic structure with a 10.2 Å unit cell (12). The cathodically deposited NiHCF electrode shown in Fig. 1a had a capacity equal to 11.5 mC/cm^2 at the 25th (final) deposition cycle, with a corresponding film thickness of 190 nm. Figure 1b shows the growth in ion-exchange capacity as a function of deposition cycle. A linear relationship persists over all 25 cycles, suggesting that film deposition could be continued further, thereby increasing the ion-exchange capacity. Of course, at some unknown thickness, the film will no longer be able to maintain electronic conductivity and growth will halt. Films have been prepared with capacities as high as 15 mC/cm^2 (corresponding to 235 nm) using no special procedures. X-ray spectra obtained from the freshly prepared film showed trace amounts of K^+ in addition to Na^+, as a result of the deposition solution containing 0.006 M K^+ in addition to 0.5 M Na^+. However, no K^+ was detected at any later stage, indicating that K^+ was fully displaced by Na^+ during oxidation and reduction in 1.0 M $NaNO_3$.

General Characteristics of Na^+/Cs^+ Loading

Figure 2 shows the typical reversible electrochemical behavior of a cathodically deposited NiHCF electrode cycled (50 times) in each of nine different electrolyte solutions with varied Cs^+/Na^+ compositions. Positive currents correspond to the oxidation of iron centers in the film, with the corresponding elution of Na^+ or Cs^+ from the matrix (see Eq. 1), whereas negative currents correspond to iron reduction and Na^+ or Cs^+ loading. This qualitative description of iron-center-redox behavior has been confirmed by in situ Raman spectroscopy (25). Thin-film NiHCF electrodes remain redox-active over several thousand load–elute cycles in electrolytes of the type used here (17).

The cyclic voltammograms in Fig. 2 illustrate the transition from predominantly Na^+ exchange to Cs^+ exchange as the cathodically deposited film is cycled in Na^+/Cs^+ mixtures with increasing amounts of Cs^+. Pure Na^+ exchange is shown in (i) and pure Cs^+ exchange is shown in (ix). The redox potential of the reversible wave depends on the ionic radius of the exchanging cation in anodically derivatized films (17). Therefore, the shift of the redox potential toward more positive values in curves (i) through (ix) qualitatively indicates an increasing amount of Cs^+ loading. Voltammograms (ii), (iii), (iv), and (v) are quite similar to (i) in redox potential, suggesting that Na^+ is the predominant cation being exchanged when [Cs^+] is between 10^{-7} and 10^{-4} M. Voltammograms (vi), (vii), and (viii) have greatly shifted redox potentials, suggesting that Cs^+ is the predominant cation being exchanged when [Cs^+] is between 10^{-3} and 10^{-1} M.

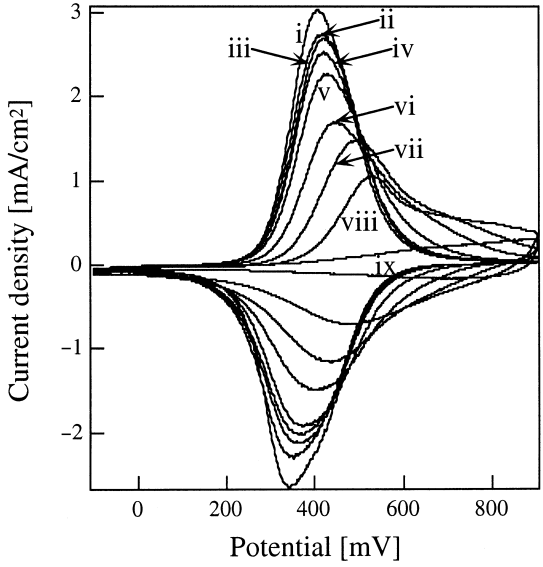

FIG. 2 Cyclic voltammograms for a NiHCF electrode cycled in a series of aqueous Na^+ and Cs^+ nitrate mixtures. All solutions had a total alkali content ($[Cs^+] + [Na^+]$) of 1 M. The Cs^+ concentration in each solution was (i) 0 M, (ii) 10^{-7} M, (iii) 10^{-6} M, (iv) 10^{-5} M, (v) 10^{-4} M, (vi) 10^{-3} M, (vii) 10^{-2} M, (viii) 10^{-1} M, and (ix) 1 M.

In addition to a shift in redox potential, the reversible ion-exchange capacity is seen to decrease dramatically in Fig. 2 as $[Cs^+]/[Na^+]$ in solution increases. Since cyclic voltammetry in pure 1.0 M $NaNO_3$ (i) or 1.0 M $CsNO_3$ (ix) results in the exclusive exchange of Na^+ or Cs^+, respectively, the molar amounts of Cs^+ or Na^+ that are exchanged when the oxidation state of the iron centers is modulated can easily be determined from the average integrated charge, Q_i, such that

$$N^*_{Na} = \frac{Q_{Na}}{F} \text{ and } N^*_{Cs} = \frac{Q_{Cs}}{F} \tag{2}$$

where F is Faraday's constant. Using the data in curves (i) and (ix), one finds $N^*_{Na} = 2.2 \times 10^{-8}$ and $N^*_{Cs} = 0.37 \times 10^{-8}$ moles. In other words, the redox ion-exchange capacity in (ix) is only 17% of the ion-exchange capacity in (i). This suggests that not all the matrix sites are available for Cs^+ exchange. To better quantify these trends in cation loading from different electrolytes, we describe the use of energy-dispersive x-ray spectroscopy as a nondestructive probe of Na^+ and Cs^+ content in the matrix.

Energy-Dispersive X-ray Spectroscopy

Energy-Dispersive X-ray Spectroscopy (EDS) probes core electronic structures, thereby allowing elemental analysis without sensitivity to valence electrons involved in chemical bonding. Figure 3 shows a typical background-subtracted spectrum acquired after the cathodically deposited NiHCF electrode was cycled 50 times in 10^{-3} M $CsNO_3$ + 0.999 M $NaNO_3$ solution. The spectrum contains peaks due to elements found in the NiHCF matrix (Ni and Fe), intercalated cations (Na and Cs), and the substrate (Pt). However, one cannot quantify species by simple inspection. For example, the difference in magnitude between the Cs L_α peak at 4.282 keV and the Na K_α peak at 1.041 keV does not directly reflect their relative content in the matrix, since Cs has much larger x-ray generation parameters (ionization cross section and fluorescence yield) than Na. Furthermore, the detector efficiency is ≈45% at 1 keV (26), whereas it is nearly 100% for energies above 2 keV. On the other hand, the Ni K_α peak at 7.471 keV and the Fe K_α peak at 6.402 keV have similar peak heights since nickel and iron have similar x-ray generation parameters and are (ideally) present in 1:1 stoichiometry in the matrix. Note that the combined Pt M_α (2.048 keV) and M_β (2.127 keV) peak in the low-energy portion of the spectrum is shown at 4% of its true magnitude. Platinum has strong x-ray generation parameters, but more importantly, it is a thick substrate covered by a layer that is thin compared to the electron beam penetration depth. Thus, most of the x-ray generation arises from the Pt substrate, not the NiHCF film. Cal-

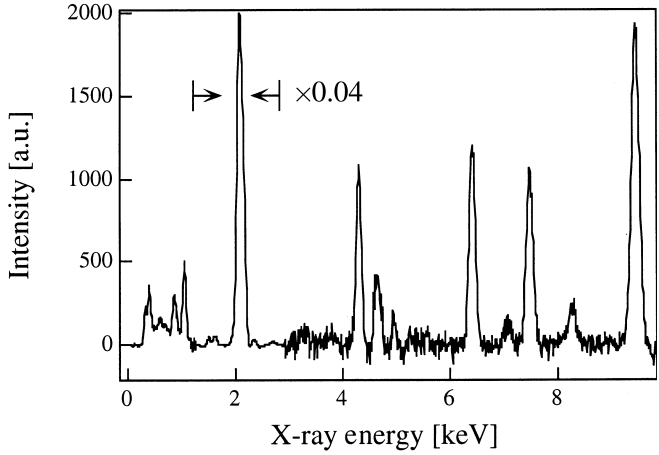

FIG. 3 Baseline subtracted energy dispersive x-ray spectrum of a NiHCF electrode loaded with cations from an aqueous solution of 10^{-3} M $CsNO_3$ + 0.999 M $NaNO_3$. Note the region near 2 keV where the intensity has been attenuated.

culations show that NiHCF electrodes used here can be considered thin films for quantitation purposes.

The theory of x-ray intensity for thin films is well developed (27–29). The measured intensity (peak height) for an element that is present only in the thin film is linearly dependent on its concentration in the film and the film thickness (29). The intensity relation for Na, Cs, Fe, or Ni can be written in the simplified form

$$I_i = k_{INST} k_{FILM,i} k_{SUBST,i} k_{PHYS,i} t[i] \quad (3)$$

where t denotes film thickness, $[i]$ denotes the atomic or molar concentration of element i, and the other quantities are correction factors to be discussed further. The constant k_{INST} accounts for instrumental factors such as detector geometry, probe current, etc. and is independent of the element measured. The factor $k_{FILM,i}$ accounts for the loss in x-ray intensity due to absorption by other elements in the film. Using a worst-case scenario, we calculate this absorption loss to be less than 10% for the elements measured here. The factor $k_{SUBST,i}$ accounts for additional x-ray intensity due to substrate fluorescence and backscattered electrons. In the limit of a thin film on a thick substrate, these effects are constant from film to film. The constant $k_{PHYS,i}$ incorporates the physics of x-ray generation, i.e., scattering cross section, fluorescence yield, etc., and can be found in the literature (26). Each of these factors will cancel one another in the subsequent analysis.

Normally, a superior standard is used to eliminate the various correction factors and obtain an absolute value for the concentration of each element. However, this procedure requires that all elements in the sample be quantified, which is not possible for the low energy C and N peaks. As an alternative, the iron centers in the NiHCF matrix can be used as an internal standard to obtain the normalized x-ray intensity ratios I_{Na}/I_{Fe} and I_{Cs}/I_{Fe}. Using Eq. (3), it is straightforward to show that the moles of cation j loaded into the reduced matrix are

$$N_j = \frac{I_j/I_{Fe}}{(I_j/I_{Fe})^{**}} N_j^{**} \quad (4)$$

where N_j^{**} represents the moles of j in the matrix when it is loaded using pure solutions of a single salt (e.g., 1.0 M $NaNO_3$), and $(I_j/I_{Fe})^{**}$ is the corresponding Fe-normalized x-ray intensity for this matrix. By using Fe as an internal standard, the effects of film thickness are eliminated as well as the effects of the four correction factors.

There is an important and subtle difference between N_j^*, defined in Eq. (2), and N_j^{**}, used in Eq. (4). The quantity N_j^* denotes the number of moles of j that load or elute during a given electrochemical redox exchange, as shown in Eq. (1). Examining Eq. (1) further shows that the optimal redox exchange

(with $x = 1$) results in half of the alkali cations being exchanged electrochemically. In contrast, N_j^{**} accounts for all the alkali cations in the reduced matrix. Thus, if species j has an optimal redox exchange where $x = 1$ in Eq. (1), then $N_j^{**} = 2N_j^*$. The large value of N_j^* for Na^+ as well as Raman spectroscopy data for anodically derivatized films (25) suggest that Na^+ can undergo redox exchange with $x \approx 1$. Assuming that $x = 1$ for Na^+, N_{Na}^{**} is twice as large as N_{Na}^*. In more general terms, the value of N_j^{**} is equal to

$$N_j^{**} = N_{Na}^* + N_j^* \tag{5}$$

Including the term N_{Na}^* in Eq. (5) properly accounts for the alkali cations that do not exchange during a given redox cycle but are nonetheless probed by EDS.

Implicit in this analysis are the assumptions that no synergistic interaction occurs between the different cations loading into the NiHCF matrix, and that the Fe content of the film remains stable as the electrode is cycled. A lack of synergistic interactions implies that the maximum amount of Cs^+ loads into the NiHCF from a pure Cs^+ solution, an assumption that is borne out by experiments. The latter assumption also seems reasonable since, on average, the absolute Fe intensity does not decrease over the hundreds of redox cycles experienced by these electrodes. From the discussion presented here and additional experimental checks, systematic errors associated with the breakdown of assumptions in the analysis are believed to be limited to less than 10% of reported values. Random errors will be represented by $\pm 1\sigma$ error bars, as determined from replicate measurements; note that in several instances, the error bars cannot be seen, as they are smaller than the data markers.

Na^+/Cs^+ Selectivity

The analysis outlined above permits us to calculate the molar content of each individual cation species loaded into the NiHCF ion-exchange matrix. To get at selectivity parameters for the NiHCF matrix, it is necessary to determine the mole fraction of Cs^+ loaded into the ion exchange matrix, i.e.,

$$Y_{Cs,MATRIX} = \frac{N_{Cs}}{N_{Cs} + N_{Na}} \tag{6}$$

Figure 4 shows $Y_{Cs,MATRIX}$ vs. $X_{Cs,SOLN,}$ where $X_{Cs,SOLN}$ is the mole fraction of Cs^+ in solution. Since each spectrum represents a single 1000×1000 μm region, we sampled multiple regions to determine average (I_{Cs}/I_{Fe}) and (I_{Na}/I_{Fe}) for each solution. Each data point in this figure is the result from six spectra that together cover ~ 1/3 of the total exchanger area. To gauge the accuracy of these measurements, two additional NiHCF electrodes (with capacities 11.3 and 11.6 mC/cm^2) were prepared and examined in pure Na^+, 10^{-3} M Cs^+ + 0.999 M Na^+, and pure Cs^+ salt solutions using higher signal-to-noise acqui-

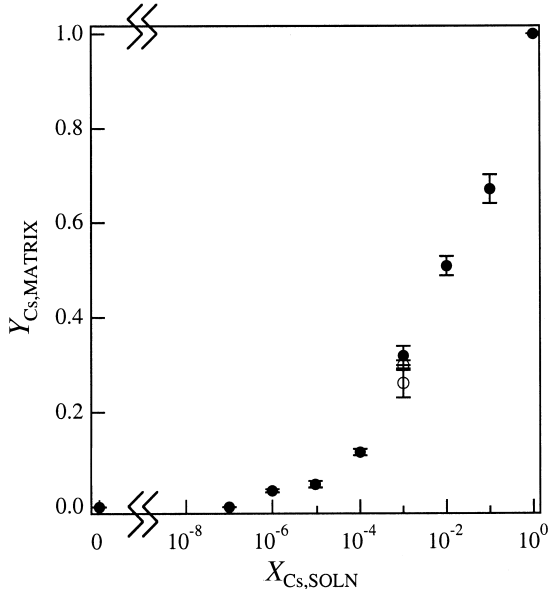

FIG. 4 Cs^+ mole fraction in the ion-exchange matrix ($Y_{Cs,MATRIX}$) as a function of the Cs^+ mole fraction in solution ($X_{Cs,SOLN}$). Additional NiHCF electrodes (o) are shown at $X_{Cs,SOLN} = 10^{-3}$.

sition conditions (15 minute accumulation times). These improved data match the original results well and suggest that within-film variation is comparable to film-to-film variation in NiHCF electrodes. Thus, multiple sampling within a single film is a reasonable method to quickly assess variation at a given solution composition.

Figure 4 quantifies the trends noted earlier in Fig. 2. $Y_{Cs,MATRIX}$ is less than 0.1 when $[Cs^+]$ is between 10^{-6} and 10^{-4} M, whereas it increases rapidly when $[Cs^+]$ is between 10^{-3} and 10^{-1} M. These results show that cathodically deposited NiHCF electrodes are indeed selective for Cs^+ over Na^+ since $Y_{Cs,MATRIX}$ greatly exceeds $X_{Cs,SOLN}$ for $[Cs^+]$ between 10^{-1} and 10^{-6} M. Note that there is no detectable Na^+ when $[Cs^+]$ is equal to 1.0 M and no detectable Cs^+ when $[Cs^+]$ is equal to 10^{-7} M. For 10 minute accumulation times, signal-to-noise considerations suggest the Na^+ and Cs^+ detection limits are approximately 4×10^{-9} and 1×10^{-9} moles, respectively, for films of the thickness probed here. Two additional NiHCF electrodes (with capacities 10.9 and 12.4 mC/cm^2) were prepared and examined using 15 and 20 minute accumulation times in pure Na^+, 10^{-7} M Cs^+ + 1 M Na^+, and pure Cs^+ salt solutions. Despite the lowered detection limits af-

forded by the longer accumulation times, no Cs^+ was detected in either film when [Cs^+] was 10^{-7} M; therefore, this concentration cannot be included in the analysis that follows.

One common way to quantify selectivity is by the separation factor

$$\alpha_{Na}^{Cs} = \frac{Y_{Cs,MATRIX}/Y_{Na,MATRIX}}{X_{Cs,SOLN}/X_{Na,SOLN}} \tag{7}$$

where $Y_{i,MATRIX}$ and $X_{i,SOLN}$ refer to the mole fractions of element i in the ion-exchange matrix and contacting electrolyte solution, respectively. Since α_{Na}^{Cs} deals with concentrations rather than activities, it is not a thermodynamic quantity. A single ion-exchange material will have very different separation factors when tested over a wide range of solution compositions. Figure 5 compares separation factor data for the anodically derivatized films reported by Rassat et al. with the cathodically deposited films described here. Both films display excellent separation factors. Furthermore, over the composition range where the films can be compared directly (i.e., $X_{Na,SOLN}/X_{Cs,SOLN}$ from 10^2 to 10^4), the anodically derivatized films have nearly identical separation factors to the cathodically deposited films. This result, though perhaps surprising owing to the sensitivity of hexacyanoferrate stoichiometry to preparation conditions (12), suggests that cathodically deposited NiHCF can achieve compara-

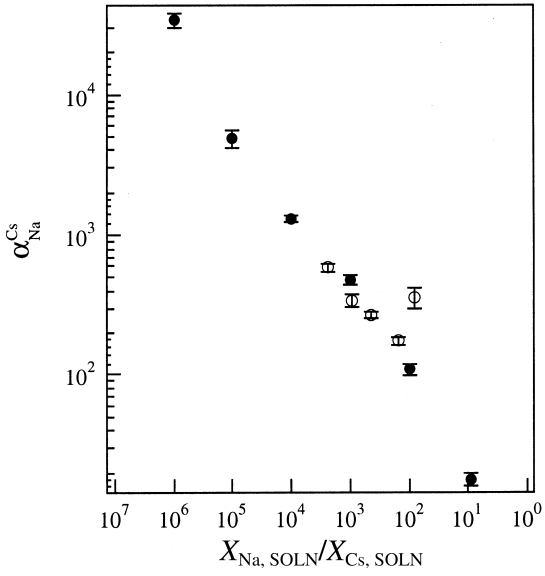

FIG. 5 Comparison of the separation factor, α, from anodically derivatized NiHCF electrodes (o) reported by Rassat et al. and cathodically deposited NiHCF electrodes (•) determined here.

ble separations to anodically derivatized NiHCF, but with higher ion-exchange capacities.

An alternative way to look at the data is by plotting the distribution coefficient, K_D, which is calculated using

$$K_D = \frac{N_{Cs}}{m[Cs^+]_{EQ}} \tag{8}$$

where $[Cs^+]_{EQ}$ is the equilibrium Cs^+ concentration in solution following exchange and m is the weight of the ion-exchange matrix. The weight of NiHCF deposited on the electrode can be estimated from electrochemical measurements during the deposition cycles. Assuming the whole film is active during deposition, Faraday's law gives

$$m = \frac{Q_G}{F} \mathrm{M}_{NiHCF} \tag{9}$$

where Q_G is the integrated charge calculated at the end of the deposition cycle and M_{NiHCF} is the molecular weight of NiHCF (taken as 271 g/mol, not including the mass of loaded cations). Determining the exchanger mass using Eq. (9) accounts for the weight of active material only and thus provides an upper bound for K_D. For the experimental conditions used here, the equilibrium concentration after exchange, $[Cs^+]_{EQ}$, is set equal to the original concentration, $[Cs^+]$, since the ion-exchange capacity of the NiHCF film is at least 10^7 times smaller than the ion content of the electrolyte volume.

Unlike α_{Na}^{Cs}, K_D can be calculated for Cs^+ exchange when there are no competing cations, thereby allowing a more transparent assessment of the role that Na^+ competition plays. Figure 6 shows experimental data for K_D plotted against $[Cs^+]_{EQ}$. These experimental values are compared to the hypothetical case of a perfect separation, as extrapolated from Cs^+ exchange where there is no Na^+ competition i.e. 1.0 M $CsNO_3$. A perfect separation occurs if all sites in the NiHCF ion-exchange matrix permit only a single cation to enter the structure, no matter how much competing cation exists. When $[Cs^+]$ is between 10^{-1} and 10^{-3} M, K_D remains fairly close to the perfect separation line, indicating that $[Na^+]$ has little effect. When $[Cs^+]$ is between 10^{-4} and 10^{-6} M, K_D falls to less than 50% of the perfect separation value, which indicates the point where sites are being filled by the competing cation Na^+. At sufficiently low concentrations of Cs^+, K_D should plateau. However, experiments at these concentrations could not be performed because the amount of Cs^+ within the matrix drops below the detection limit of the spectrometer (for the accumulation times used). Quantitation of Cs^+ at these lower concentrations might be possible using XPS with sputtering, or SIMS, but those possibilities have not been explored in depth.

There have been numerous studies with bulk hexacyanoferrate materials, which can be used to gauge the performance of cathodically deposited Ni-

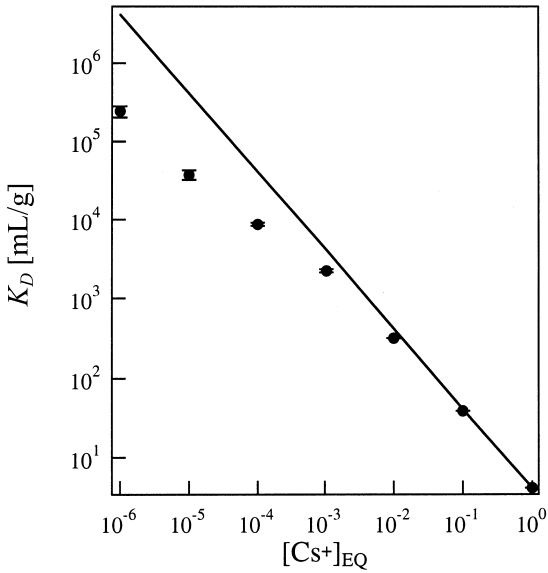

FIG. 6 Experimentally measured distribution coefficients (•) compared to a hypothetical perfect separation (—) where only Cs^+ is permitted to intercalate into the ion-exchange matrix.

HCF electrodes. For solution compositions that are relevant to these studies, one finds that most bulk metal hexacyanoferrates (e.g., nickel, cobalt, copper, zinc, tungsten, and uranium ferrocyanide compounds) have K_D values that plateau in the range from 10^4 ml/g to 10^5 ml/g (4, 7, 10, 11, 13, 30–32), with some nickel, cobalt, and zinc hexacyanoferrate values being reported as high as 5×10^5 ml/g (4, 11, 32). Previous studies with bulk hexacyanoferrates also make clear that Na^+ competition is expected to have little effect on K_D for Cs^+. The data in Fig. 6 for the cathodically deposited NiHCF electrode show that K_D is equal to 2.5×10^5 ml/g for $[Cs^+] = 10^{-6}$ M and $[Na^+] \approx 1$ M, and it has not yet plateaued. Our results for cathodically deposited NiHCF electrodes appear to match the performance of most bulk hexacyanoferrate materials.

Electrochemical Regeneration of the Ion-Exchange Matrix

Thus far only loading characteristics of the cathodically deposited NiHCF electrode have been considered. Recall that one of the main problems with bulk hexacyanoferrate exchange is that there is no simple way to thoroughly regenerate the ion-exchange matrix once it is in the Cs-form without material degradation. One advantage of electrochemically switched ion exchange is that the additional electrochemical driving force might allow matrix regener-

ation, hence a multiple use material. Figure 7 shows qualitatively that regeneration of the ion-exchange matrix from the Cs-form to the Na-form can be accomplished by cycling a Cs-loaded film in a Na^+-containing electrolyte. The voltammograms show an immediate shift in redox potential and increased ion-exchange capacity, suggesting a return to primarily Na^+ exchange. Voltammogram (ii) has 70% as much ion-exchange capacity as voltammogram (i) in Fig. 2. From voltammogram (ii) to (v) there is less than 10% additional capacity gain. Not only does it appear that we can electrochemically regenerate the NiHCF film to the Na-form, but we do so without degrading the material (as evidenced by a significant recovery of capacity).

Despite the apparent electrochemical regeneration displayed in Fig. 7, the best evidence is direct measurement of the cation content of the NiHCF film. Figure 8 shows $Y_{Cs,MATRIX}$ as a function of redox cycles in 1.0 M $NaNO_3$. The figure also shows $Y_{Cs,MATRIX}$ for an additional, chemically regenerated NiHCF electrode; this Cs-loaded film was held at −100 mV vs SCE for times equivalent to 50 redox-cycle increments. The data in Fig. 8 were acquired by x-ray spectroscopy following each 50 cycles or equivalent time, and each data point is the result from three spectra that together cover ~ 1/6

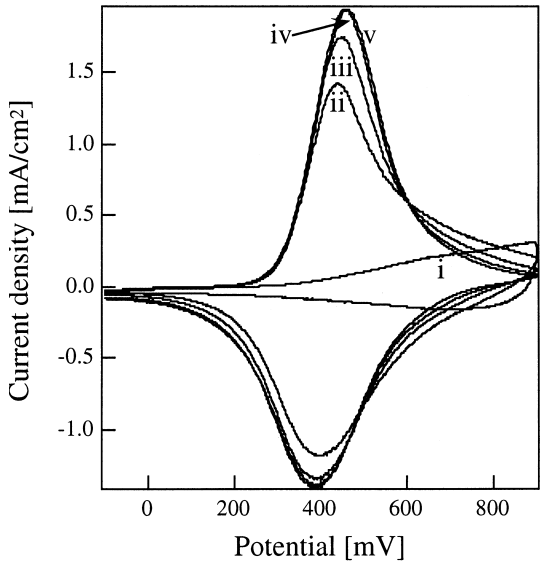

FIG. 7 Cyclic voltammograms showing matrix regeneration by potential cycling a Cs-loaded film in 1 M $NaNO_3$. Curve (i) corresponds to the 50th cyclic voltammogram acquired in 1 M $CsNO_3$ [same as curve (ix) in Fig. 2]. For curve (ii), the Cs-loaded film is cycled 50 times in 1 M $NaNO_3$, then removed for acquisition of x-ray spectra. For curves (iii)–(v), this process is repeated in fresh 1 M $NaNO_3$.

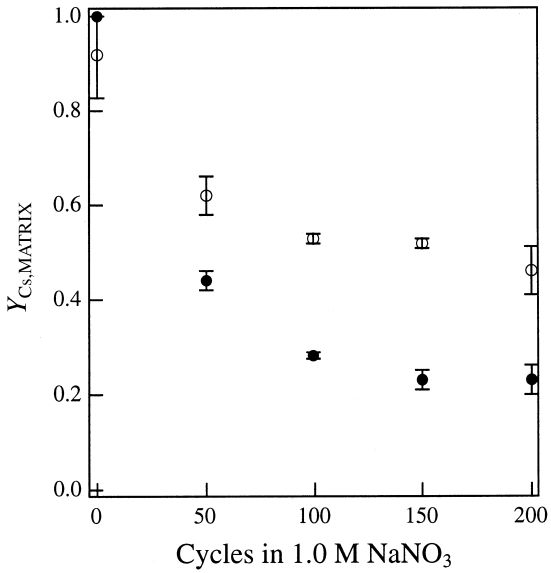

FIG. 8 Cs^+ mole fraction in the ion-exchange matrix ($Y_{Cs,MATRIX}$) as Cs-loaded films are regenerated in 1 M $NaNO_3$ by electrochemical or chemical means. Electrochemical regeneration data (•) correspond to curves (i) through (v), respectively, in Fig. 7. Chemical regeneration data (o) are from a Cs-loaded film held at −100 mV vs SCE in fresh 1 M $NaNO_3$ for times equivalent to 50 redox cycle increments.

of the exchanger area. The electrochemical regeneration data in Fig. 8 show a large change in Cs^+ content within the first 50 cycles; at 200 cycles, $Y_{Cs,MATRIX}$ seems to be steady at ≈0.23. Surprisingly, the chemical regeneration data in Fig. 8 show that Na^+ can partially displace Cs^+ via a purely chemical regeneration step, such that the final $Y_{Cs,MATRIX}$ value is ≈0.46. Overall, the amount of Cs^+ remaining after electrochemical regeneration is half what remains after chemical regeneration.

An adequate volume of regeneration solution was used to ensure that the concentration of Cs^+ remained sufficiently small after elution to avoid reloading the Cs^+ in subsequent cycles. Given this, the fact that $Y_{Cs,MATRIX} \approx 0.23$ after electrochemical regeneration in 1.0 M $NaNO_3$ suggests that a small portion of Cs^+ is irreversibly trapped in the ion-exchange matrix. This irreversibly trapped portion may play a role in the eventual cycle-life degradation of the material. Cycle-life degradation is the subject of continuing study. It is interesting that some chemical regeneration was observed, since bulk NiHCF will not elute appreciable amounts of Cs^+ without harsh treatment. The observation that NiHCF thin films can be partially regenerated by soaking in

Na^+ containing electrolyte points to possible transport effects in bulk materials that hinder their regeneration.

CONCLUSIONS

It has been demonstrated that cathodically deposited nickel hexacyanoferrate thin-film electrodes are suitable for electrochemically switched ion-exchange processes. Potential modulation results in a nearly reversible exchange of cations that can be sustained over many oxidation/reduction cycles. The materials studied here are highly selective to Cs^+ loading for $[Cs^+] = 10^{-1}$ to 10^{-6} M. The distribution coefficient ($K_D > 10^5$ ml/g) for 10^{-6} M Cs^+ in the presence of $\approx$1 M Na^+ was similar to those from bulk hexacyanoferrates. The main advantage of thin-film nickel-hexacyanoferrate electrodes over bulk hexacyanoferrates is they provide a means (potential modulation) to regenerate the ion-exchange material without chemicals or significant matrix degradation. However the entire matrix cannot necessarily be regenerated. We are currently investigating whether film preparation can be altered to increase Cs^+ selectivity, ion-exchange capacity, regenerability, and cycle life.

ACKNOWLEDGMENTS

This work was supported by the Department of Energy's Environmental Management Science Program. K. M. J. acknowledges the support provided by a National Science Foundation Graduate Research Fellowship, and D. T. S. thanks Professor Dieter Landolt at the École Polytechnique Fédérale de Lausanne for sabbatical leave support provided during the preparation of this manuscript. The authors would like to thank one of the anonymous reviewers for their insightful comments that led to important improvements in the EDS analysis.

REFERENCES

1. M. A. Lilga, R. J. Orth, J. P. H. Sukamto, S. M. Haight, and D. T. Schwartz, *Sep. Pur. Tech., 11,* 147 (1997).
2. S. D. Rassat, J. P. H. Sukamto, R. J. Orth, M. A. Lilga, and R. T. Hallen, *Ibid., 15,* 207 (1999).
3. V. Pekarek and V. Vesely, *Talanta, 19,* 1245 (1972).
4. D. O. Campbell, D. D. Lee, and T. A. Dillow, *ORNL/TM-11798* (1991).
5. P. A. Haas, *Sep. Sci. Technol., 28,* 2479 (1993).
6. R. Harjula, J. Lehto, E. H. Tusa, and A. Paavola, *Nucl. Technol., 107,* 272 (1994).
7. J. Krtil, *Radiochim. Acta, 7,* 30 (1967).
8. E. F. T. Lee and M. Streat, *J. Chem. Technol. Biotechnol., 33A,* 333 (1983).
9. C. Loos-Neskovic and M. Fedoroff, *Radioact. Waste Manag., 11,* 347 (1989).
10. W. E. Prout, E. R. Russel, and H. J. Groh, *J. Inorg. Nucl. Chem., 27,* 473 (1965).

11. S. Vlasselaer, W. D'Olieslager, and M. D'Hont, *J. Inorg. Nucl. Chem., 38,* 327 (1976).
12. C. Loos-Neskovic and M. Fedoroff, *Solvent Extr. Ion Exch., 7,* 131 (1989).
13. E. F. T. Lee and M. Streat, *J. Chem. Technol. Biotechnol., 33,* 80 (1983).
14. L. J. Amos, A. Duggal, E. J. Mirsky, P. Ragonesi, A. B. Bocarsly, and P. A. F. Bocarsly, *Anal. Chem., 60,* 245 (1988).
15. D. R. Coon, L. J. Amos, A. B. Bocarsly, and P. A. F. Bocarsly, *Ibid., 70,* 3137 (1998).
16. B. D. Humphrey, S. Sinha, and A. B. Bocarsly, *J. Phys. Chem., 91,* 586 (1987).
17. S. Sinha, B. D. Humphrey, and A. B. Bocarsly, *Inorg. Chem., 23,* 203 (1984).
18. S. Sinha, B. D. Humphrey, E. Fu, and A. B. Bocarsly, *J. Electroanal. Chem., 162,* 351 (1984).
19. J. Bacskai, K. Martinusz, E. Czirok, G. Inzelt, P. J. Kulesza, and M. A. Malik, *Ibid., 385,* 241 (1995).
20. L. F. Schneemeyer, S. E. Spengler, and D. W. Murphy, *Inorg. Chem., 24,* 3044 (1985).
21. A. B. Bocarsly and S. Sinha, *J. Electroanal. Chem., 140,* 167 (1982).
22. S. J. Lasky and D. A. Buttry, *J. Amer. Chem. Soc., 110,* 6258 (1988).
23. A. B. Bocarsly and S. Sinha, *J. Electroanal. Chem., 137,* 157 (1982).
24. X. Zeng, S. Moon, S. Bruckenstein, and A. R. Hillman, *Anal. Chem., 70,* 2613 (1998).
25. S. M. Haight, D. T. Schwartz, and M. A. Lilga, *J. Electrochem. Soc., 145,* 1866 (1999).
26. J. I. Goldstein, D. E. Newbury, P. Echlin, D. C. Joy, A. D. R. Jr., C. E. Lyman, C. Fiori, and E. Lifshin, *Scanning Electron Microscopy and X-ray Microanalysis,* Plenum Press, New York, 1992.
27. M. G. C. Cox, G. Love, and V. D. Scott, *J. Phys. D, 12,* 1441 (1979).
28. G. A. Hutchins, *The Electron Microprobe* (McKinley, et al., Eds.), Wiley & Sons, New York, 1966.
29. P. Willich, *Mikrochim. Acta, 12,* 1 (1992).
30. J. Krtil, *J. Inorg. Nucl. Chem., 27,* 233 (1965).
31. J. Lehto, R. Harjula, and J. Wallace, *J. Radio. Nuc. Chem., 111,* 297 (1986).
32. J. Lehto and R. Harjula, *Solvent Extr. Ion Exch., 5,* 343 (1987).

Received by editor August 10, 1999
Revision received October 1999